https://doi.org/10.5194/egusphere-2023-1010
Preprint. Discussion started: 9 June 2023

Ambient methane monitoring at Hohenpeißenberg utilizing photoacoustic spectroscopy and cavity ring down spectroscopy

Max Müller[1, 2], Stefan Weigl[1], Jennifer Müller-Williams[3], Matthias Lindauer[3], Thomas Rück[1], Simon Jobst[1, 2], Rudolf Bierl[1], and Frank-Michael Matysik[2]

[1]Sensorik-ApplikationsZentrum, University of Applied Sciences Regensburg, 93053 Regensburg, Germany
[2]Institute of Analytical Chemistry, Chemo- and Biosensors, University Regensburg, 93053 Regensburg, Germany
[3]Meteorological Observatory Hohenpeißenberg, Deutscher Wetterdienst, 82383 Hohenpeißenberg, Germany

Correspondence: Max Müller (max.mueller@oth-regensburg.de)

Abstract. With an atmospheric concentration of approximately 2000 parts per billion (ppbV, 10^{-9}) methane (CH_4) is the second most abundant greenhouse gas (GHG) in the atmosphere after carbon dioxide (CO_2). The task of long-term and spatially resolved GHG monitoring to verify whether climate policy actions are effective, is becoming more crucial as climate change progresses. In this paper we report the CH_4 concentration readings of our photoacoustic (PA) sensor over a five day period at Hohenpeißenberg, Germany. As a reference device a calibrated cavity ringdown spectrometer Picarro G2301 from the meteorological observatory was employed. Trace gas measurements with photoacoustic instruments promise to provide low detection limits at comparably low costs. However, PA devices are often susceptible to cross-sensitivities related to environmental influences. The obtained results show that relaxation effects due to fluctuating environmental conditions, e.g. ambient humidity, are a non-negligible factor in PA sensor systems. Applying algorithm compensation techniques, which are capable of calculating the influence of relaxational effects on the photoacoustic signal, increase the accuracy of the photoacoustic sensor significantly. With an average relative deviation of 1.11 % from the G2301, the photoacoustic sensor shows good agreement with the reference instrument.

1 Introduction

In the European network Integrated Carbon Observation System (ICOS) 16 different nations united to measure greenhouse gas (GHG) concentrations continuously in the atmosphere and in a standardized way. In order to ensure data comparability of the 46 atmosphere monitoring stations the required accuracy of the devices were defined in the ICOS program. For CH_4 this was specified to be less than ± 2 ppbV, emphasising the high standards set internationally for reliable atmospheric GHG monitoring. For this purpose a state-of-the-art cavity ringdown spectrometer G2301 (Picarro, Inc.,USA) was selected by the ICOS program for both CH_4 and CO_2 quantification, which provides a 3σ precision for CH_4 less than 1.5 ppbV and less than 210 ppbV for CO_2 at an averaging time of 5 seconds.

For leakage detection of gas pipelines, or identification of various methane sources, measurement instruments with slightly lower precision may also be appropriate. In 2021 Defratyka et al. identified several sources of methane emission in Paris,

https://doi.org/10.5194/egusphere-2023-1010
Preprint. Discussion started: 9 June 2023

which increased the CH_4 concentration by up to 2.7 parts per million (ppmV, 10^{-6}), compared to the average background of about 2 ppmV (Defratyka et al., 2021). The highest emission was assigned to a ventilation grid, which increased the CH_4 concentration by about 40 ppmV. Elevations of CH_4 levels up to 88.6 ppmV were measured in Washington in 2014 by Jackson et al. (2014). This work reported a total of 5893 pipeline leaks over a distance of 1500 road miles, from which 1122 leaks increased the ambient CH_4 concentration to more than 5 ppmV and 67 leaks even over 25 ppmV. The threshold for leakage identification was proposed by von Fischer et al. who defined a 10% increase over the normal background concentration as a leakage (von Fischer et al., 2017). For a typical background concentration of about 2 ppmV, this corresponds to 200 ppbV. As an alternative to elaborate measurements in cities, low-cost devices with suitable CH_4 resolution (< 200 ppbV) could be installed at multiple locations and combined to a sensor network, which allows remote leakage detection. Photoacoustic (PA) gas sensors could meet these requirements of low-cost devices while retaining low enough detection limits. In PA the signal originates from converting vibrational energy of molecules into kinetic energy. A modulated light source electromagnetically excites the analyte of interest. The modulation can either be performed by amplitude modulation or wavelength modulation. Through collisions with surrounding molecules, the excited analyte molecules can release their additional vibrational energy as kinetic (translational) energy into the sample gas. This process is called vibrational-translational (VT) relaxation. The VT energy transfer increases the kinetic energy of the sample gas, causing the temperature to rise above its equilibrium value. Due to the modulation of the light source, the heat input induced by VT relaxation is also periodic, resulting in periodic density fluctuations, which per definition corresponds to a sound wave. By designing the optical path as an acoustic resonator, e.g. a cylindrical resonator, the photoacoustic sound wave can be amplified and filtered. The sound pressure linearly depends on the analyte concentration and may be detected by an acoustic-electric transducer, e.g. a microphone, quartz tuning fork (QTF) or a cantilever. Generally, the photoacoustically generated sound pressure p_{PA} for cylindrical resonators, excited in their first longitudinal mode can be described as follows (Miklós et al., 2001; Rück et al., 2023):

$$p_{\mathrm{PA}} = (\gamma - 1)\,\frac{Q}{f_{\mathrm{res}}}\,\frac{1}{2\pi^2 r^2}\,\frac{\mathrm{N_A}}{V_{\mathrm{mol}}}\,N_{\mathrm{i}}\sigma_{\mathrm{i}}(\lambda)\,P_0\varepsilon_{\mathrm{relax}} \tag{1}$$

The adiabatic exponent γ contains the number of all degrees of freedom (rotational, vibrational, translational) of the sample gas actively participating in sound propagation. Acoustic cross-sensitivities of the PA signal can be described by the ratio of the quality factor Q and the frequency f_{res} of acoustic resonance amplification. While r represents the radius of the resonator tube, $\mathrm{N_A}$ is the Avogadro constant, V_{mol} the molar volume of the sample gas, and N_{i} is the dimensionless volume ratio of the analyte with an absorption cross-section σ_{i} at the emitted wavelength λ. The emitted optical power of the light source is designated as P_0. The efficiency of non-radiative relaxation is considered by $\varepsilon_{\mathrm{relax}}$, which is a quantity between 0 and 1. This quantity depends on the efficiency of the individual energy transitions involved in the relaxation process (Hunter et al., 1974). For an accurate description of the overall relaxation cascade in case of mid-infrared (MIR - 2968.4 $\mathrm{cm^{-1}}$) methane monitoring in ambient air, i.e. mainly containing N_2, O_2 and H_2O, a total of 29 individual energy transitions have to be considered, according to Müller et al. (2022).

Regarding photoacoustic methane detection Elefante et al. developed a methane sensor based on a quantum cascade laser (QCL) emitting with an optical power of 128 mW at 1297 $\mathrm{cm^{-1}}$ (Elefante et al., 2019). With this sensor, they were able to

https://doi.org/10.5194/egusphere-2023-1010
Preprint. Discussion started: 9 June 2023

achieve a detection limit of 18 ppbV for a lock-in time (τ_{LIA}) of 100 ms. One year later in 2020, Elefante et al. reported a MIR photoacoustic methane sensor (Elefante et al., 2020). At an excitation wavenumber of 2988.8 cm^{-1} and an emitted optical power of 12.5 mW, a limit of detection (LoD) of 180 ppbV was obtained with a τ_{LIA} of 200 ms. Giglio et al. pursued a different approach regarding photoacoustic methane detection (Giglio et al., 2020). Instead of on-peak detection, they employed an array consisting of 32 QCLs covering the spectral range from 1190 to 1340 cm^{-1}. From the area underneath the measured spectrum, the methane concentration was determined with an LoD of 200 ppbV at τ_{LIA} of 10 s. In the near-infrared (NIR), Gong et al., Xiao et al. and Li et al. obtained CH_4 LoDs of 9 ppbV, 36.45 ppbV, and 177 ppbV at 500 s and 1 s lock-in time, respectively (Gong et al., 2021; Xiao et al., 2022; Li et al., 2022). The LoD of the sensor used in this work was determined to be 6.8 ppbV at τ_{LIA} = 2 s by Pangerl et al. (2022), although with a slightly higher optical power of 10.8 mW compared to the 7.5 mW emitted in this work. This decrease in optical power can be attributed to deterioration processes of the light source.

In this work we present the results of a five day CH_4 measurement campaign in ambient air at Hohenpeißenberg using a G2301 cavity ringdown spectrometer as a reference. Due to the naturally occurring fluctuations in ambient humidity during the measurement series, the relaxational behavior was significantly affected. Without including the algorithm CoNRad for data evaluation, no reasonable conclusions about the CH_4 concentration would be possible by the PA sensor. Relaxational effects are omnipresent in photoacoustic spectroscopy, e.g. Wysocki et al. (2006); Kalkman and van Kesteren (2008); Hayden et al. (2020); Lang et al. (2020); Qiao et al. (2022). Especially CH_4 is well-known to be prone to relaxational effects (Schilt et al., 2006; Barreiro et al., 2011, 2012; Elefante et al., 2020; Menduni et al., 2020; Li et al., 2020; Dello Russo et al., 2021; Müller et al., 2022; Pangerl et al., 2022; Rück et al., 2023). The intention of this paper is to demonstrate that the developed PA sensor in combination with CoNRad provides an appropriate choice for reliable and ppbV-level-precise GHG monitoring.

2 Experimental

2.1 Photoacoustic sensor

An interband cascade laser (ICL) emitting at 2968.4 cm^{-1} with an optical power of 7.5 mW, exciting the ν_{s1} stretching mode of CH_4 (absorption cross-section $\sigma_{CH_4} = 4.9{\cdot}10^{-19}$ $\mathrm{cm}^2\mathrm{mol}^{-1}$) was employed (Pangerl et al., 2022; Müller et al., 2022; Rück et al., 2023). Temperature, pressure and humidity within the PA cell were monitored by a BME280 (Bosch, Germany) TpH sensor. The PA cell is temperature controlled to 40 °C. For photoacoustic methane measurements in ambient air, relaxational effects induced by oxygen and water must be considered (Müller et al., 2022). In Figure 1(a) the overall relaxation efficiency $\varepsilon_{\mathrm{relax}}$ at an acoustic frequency of 5055 Hz for methane diluted in air is plotted against continuous humidification of the sample. The data shown in Figure 1 was obtained via CoNRad (Müller et al., 2022). In dry air $\varepsilon_{\mathrm{relax}}$ is only approximately 5.8 %, which implies that 94.2 % of the theoretically possible PA signal is lost due to delayed relaxation. The relaxation loss in case of methane in dry air is attributed to the strong coupling of the bending modes of methane ($2\nu_{\mathrm{b,CH_4}}$ = 2844 cm^{-1} and $\nu_{\mathrm{b,CH_4}}$ = 1422 cm^{-1}) with the vibrational state of oxygen ν_{O_2} = 1556 cm^{-1} (Schilt et al., 2006; Barreiro et al., 2011). This results in a fast vibrational-vibrational (VV) energy transfer from CH_4 to O_2. Oxygen, however, relaxes rather slow, causing the energy to accumulate in ν_{O_2}, and not contributing to PA signal generation, yielding a decrease of $\varepsilon_{\mathrm{relax}}$ (Schilt et al., 2006; Barreiro et al.,

https://doi.org/10.5194/egusphere-2023-1010
Preprint. Discussion started: 9 June 2023

2011; Müller et al., 2022; Pangerl et al., 2022). The addition of humidity significantly increases the relaxation efficiency due to a fast VV energy transfer from ν_{O_2} to ν_{H_2O} = 1595 cm^{-1}, followed by a fast VT relaxation (Barreiro et al., 2012; Müller et al., 2022; Pangerl et al., 2022). The frequency dependency of the relaxation efficiency for methane is shown in Figure 1(b). The graphs demonstrate that with rising acoustic frequencies the relaxation losses become much more pronounced, yielding lower PA signals and thus worse LoDs.

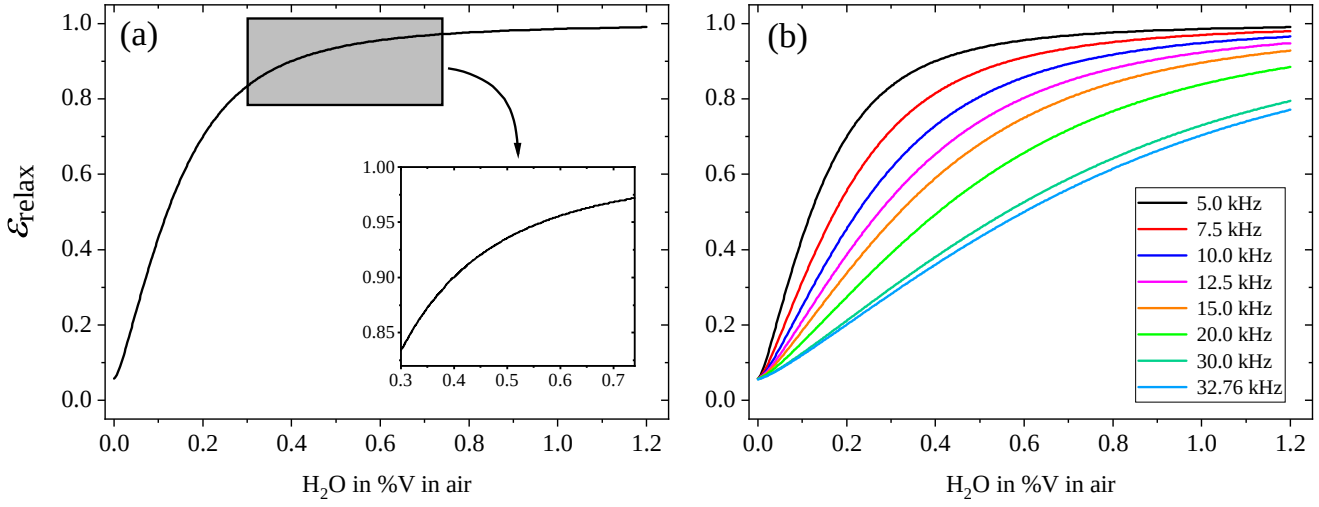

Figure 1. Overall efficiency of non-radiative relaxation ε_{relax} at 5055 Hz laser modulation for CH_4 in air with rising humidity content (a). The grey highlighted area in (a) indicates the observed humidity during the measurement period at the DWD. The right side (b) displays how humidification of the sample affects ε_{relax} at different acoustic frequencies up to 32.76 kHz, which is a typical modulation frequency utilized in quartz-enhanced PA sensors (QEPAS).

The PA sensor used in this work was operated in WM(2f) mode, i.e. the modulation frequency equals half the resonance frequency of the PA system. To prevent signal losses due to a mismatch of f_{res} and f_{mod}, the resonance properties of the PA sensor must be determined. Changes in the sample gas composition induces a change in f_{res}, as the speed of sound changes. With the acoustic resonance monitoring system (ARMS) as presented in Rück et al. (2023) an integrated, fast and accurate quantification of the acoustic properties of PA cells was introduced and utilized in this work. This technique additionally allows for Q - factor quantification, which directly affects the generated PA pressure p_{PA}, see equation 1.

https://doi.org/10.5194/egusphere-2023-1010
Preprint. Discussion started: 9 June 2023

2.2 Measurement setup

The measurement setup is visualized by Figure 2. Ambient air was sampled by means of a pump from outside the laboratory. A three-way valve was used to automatically switch between target gas and ambient air. A mixture of 2020 ppbV CH_4 and 312 ppmV CO_2 diluted in dry natural air was chosen as target gas. During the measurement campaign, the target gas was used a total of seven times for 30 minutes per interval to avoid and detect potential sensor drifts. In order to enhance the humidity during target gas operation and thus increase the generated PA signal by minimizing the influence of relaxation effects a self-developed humidity generator was installed upstream of the PA sensor (Müller et al., 2022). A lock-in-amplifier (LIA) time constant of τ_{LIA} = 20 s was chosen to reduce the effect of white noise on the PA data. Every 10 minutes the PA sensor recorded three single point measurements (SPMs) each for 20 s with a data acquisition rate of 5 Hz. The three SPMs themselves where further averaged, as well as the individual standard deviations, yielding the final values.

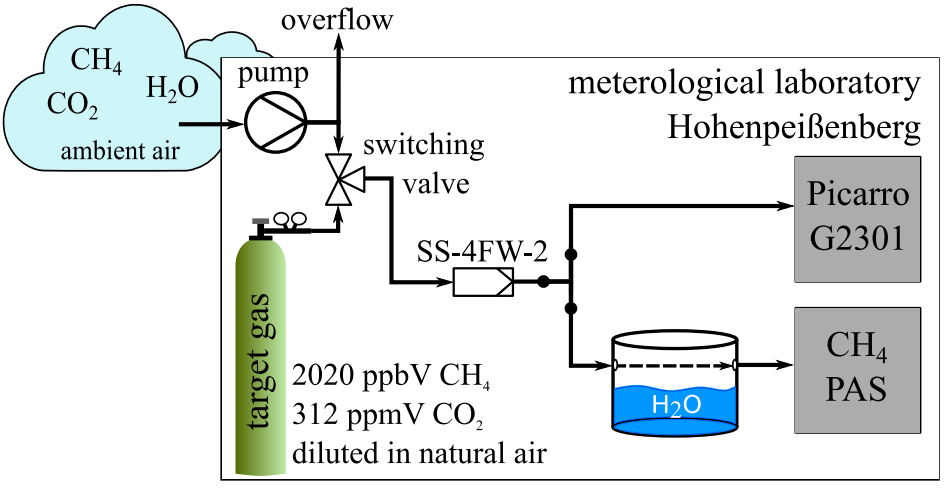

Figure 2. Schematic of the experimental setup for the measurement campaign. The pump delivers ambient air from outside the laboratory. A three-way valve is used to switch between ambient air and target gas. The target gas consists of 2020 ppbV methane and 312 ppmV carbon dioxide diluted in dry air. Before the respective sample gas is fed into the two measurement instruments, it passes a stainless steel filter (SS-4FW-2) to avoid particle contamination.

The ARMS routine was performed to determine Q and f_{res} each time before the three SPMs were recorded. Based on the ARMS, the modulation frequency of the laser was automatically adjusted, while the PA ICL was switched off between the measurements. As shown in Figure 2 the G2301 was installed in the gas setup parallel to the PA sensor, ensuring that both devices received the same sample gas, providing comparability of the sensor readings.

https://doi.org/10.5194/egusphere-2023-1010
Preprint. Discussion started: 9 June 2023

3 Results and discussion

The data of the PA sensor during target gas measurements are summarized in Table 1. The sensitivity of the PA sensor varies only slightly (maximum -2.61 % from the average value), which demonstrates the stability of the photoacoustic system. While the mean CH_4 precision $3\sigma_{PAS}$ = 6.75 ppbV is worse than the observed precision of the reference ($3\sigma_{G2301}$ = 1.16 ppbV), the PA sensor is nevertheless sufficiently precise to reliably detect the atmospheric CH_4 fluctuations, refer to Figure 3(a).

date and time	PAS sensitivity in μV/ppmV	3σ precision in nV	3σ precision in ppbV
07.02.2023 01:45	2.08	14.14	6.80
07.02.2023 09:45	2.12	22.50	10.61
08.02.2023 00:45	2.13	7.18	3.37
08.02.2023 12:45	2.16	8.59	3.98
08.02.2023 23:45	2.14	17.91	8.37
09.02.2023 11:45	2.16	14.93	6.91
09.02.2023 22:45	2.15	15.56	7.24

Table 1. Sensitivity of the PA sensor over the five day measurement period. An average deviation of 0.98 % and a maximum deviation of -2.61 % from the mean of the observed sensitivities show the stability of the PA sensor. The campaign started on 6 February 2023 afternoon and ended on 10 February 2023 morning.

Figure 3 illustrates the CH_4 readings in ppbV (a) measured by the PA sensor (black) and with the G2301 data (red), respectively. The grey dashed lines indicate a new day. It is obvious, that the CH_4 concentration characteristics monitored with both devices agree quite well with each other. However, more significant discrepancies up to > $\pm$80 ppbV, are also evident. As of now no clear explanation could be identified for these deviations. It is unlikely that these errors are induced by differences in the sample gas of the two systems since the humidity readings of the BME280 integrated in the PA sensor match very well with the readings of the G2301, as shown in Figure 3(c). By evaluating the data acquisition system (DAS), cavity, and etlaton temperature of the Picarro G2301 temporal anomalies regarding CH_4 discrepancies could be identified (see Figure A1). Since the temperature spikes are probably caused by direct sunlight on the G2301, it is recommended to avoid this for similar experiments. Still, the average percentage deviation of the PA sensor and the G2301 reference of 1.11 % is rather moderate, see Figure 3(b).

Over the entire period of the measurement campaign, the water content in the PA sample gas varied from about 0.30 %V to about 0.73 %V, see Figure 3(c), causing the PA sensor reading to alter by about 13.5 % due to relaxational effects, refer to (Figure 1(a)), which makes standard calibration unfeasible. For this reason, algorithmic compensation methods like CoNRad are essential. Figure 4 illustrates the impact of CoNRad on the reliability of PA sensor readings. The y-axis represents the difference between the CH_4 concentration readings of the PA sensor and that of the G2301 in ppbV. The grey dashed lines again indicate a new day. The black curve in Figure 4(a) shows the deviation when CoNRad is implemented ($\Delta CH_4\,(PA_{CoNRad} - G2301)$) in

https://doi.org/10.5194/egusphere-2023-1010
Preprint. Discussion started: 9 June 2023

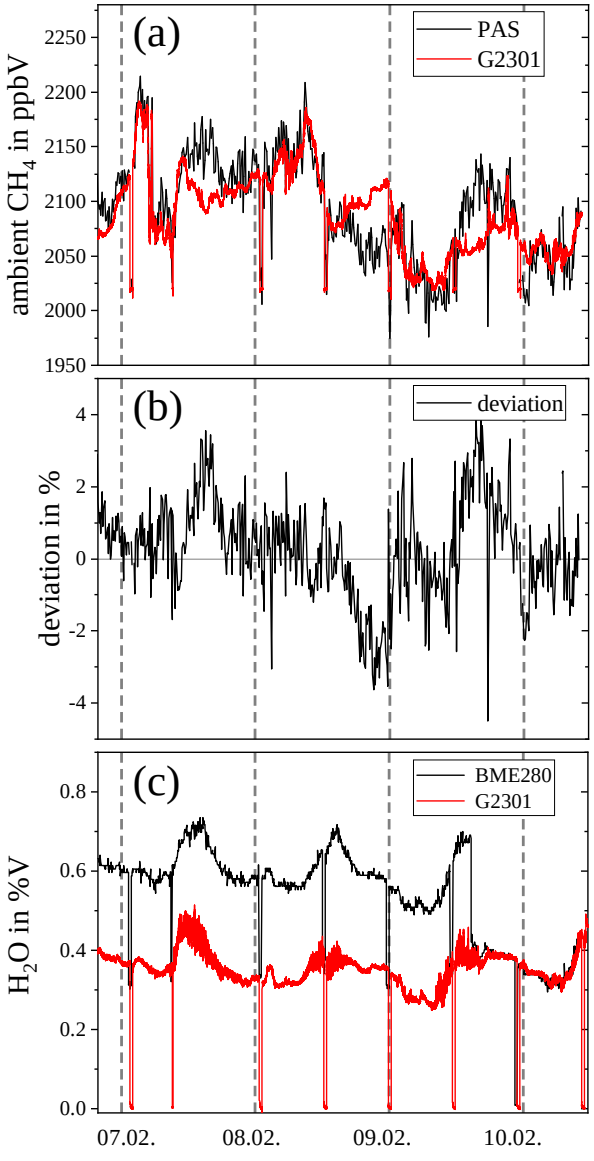

Figure 3. Direct comparison of the methane concentration readings (a), the deviation of the PA sensor compared to the Picarro G2301 in % (b) and the water readings (c). The humidity offset induced by the measurement setup is clearly visible. During 09.02. the humidity tank became empty, resulting in no additional humidification.

the data evaluation, the red curve illustrates the deviation based on the raw PA data ($\Delta CH_4\,(PA_{raw} - G2301)$). This red curve illustrates, that due to the exponential effect of relaxation processes, the offset between raw data and the reference measurement is not constant. The grey highlighted data in Figure 4 show the results for dry PA target gas operation, with the empty humidity tank during 9 February. Without CoNRad dry calibration leads to considerable misinterpretations of the PA data. Thus

https://doi.org/10.5194/egusphere-2023-1010
Preprint. Discussion started: 9 June 2023

ambient CH_4 PAS monitoring without algorithmic compensation approaches is not possible. Figure 4(b) shows a statistical evaluation of the absolute differences. It indicates that with CoNRad the variance of the measured deviation with respect to the reference decreases significantly. In addition, the compensated values show normal distribution around 5.26 ppbV, indicating no long-term drift. The raw values, however, are not normally distributed and show a substantially higher variance. The large deviation of about 1000 ppmV CH_4 of the raw PA data (grey highlighted area) can be attributed to dry target gas mode, in which pronounced relaxational losses occur, see Figure 1.

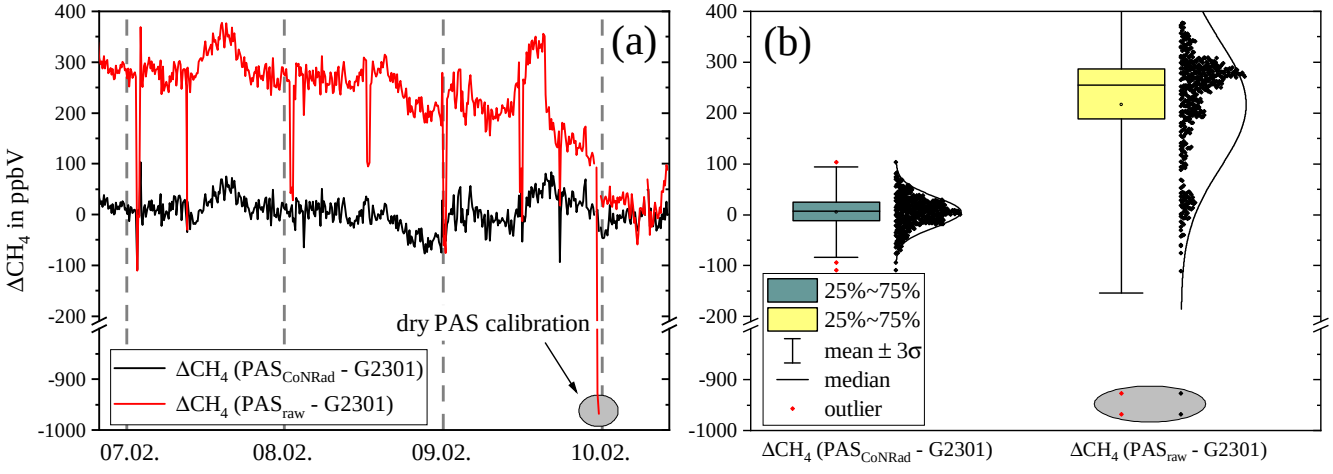

Figure 4. Absolute difference of CH_4 in ppbV (a) based on raw PA data (red) and after CoNRad compensation (black) with regard to the G2301 reference methane readings. The right side (b) displays the boxplots and histograms of the deviations. The grey highlighted data indicates dry PAS calibration without CoNRad compensation.

4 Conclusions

We compared our PA methane gas sensor with an established and calibrated cavity ringdown spectrometer (G2301) used for global GHG monitoring. Over a period of five days, ambient air has been monitored at the meteorological observatory Hohenpeißenberg of the DWD by both systems. The obtained results demonstrate that the PA sensor (3σ precision = 6.75 ppbV) is able to detect even small natural methane fluctuations in ambient air, thus providing an alternative to established devices. Further applications of the sensor would cover natural gas leakage detection, identification of new methane sources, or emission monitoring from agriculture or landfills. Generally photoacoustic systems provide low detection limits and high potential for miniaturization, however, relaxation-induced signal alterations pose a major drawback of this technique. The counteracting water and oxygen induced relaxation effects play an important role in ambient photoacoustic methane detection, as highlighted in this work. Only in environments with clearly defined and constant measurement matrix, e.g. contamination measurement of high purity gases, the effect of relaxation on the photoacoustic signal may be neglected. For complex and highly fluctuating environments, i.e. ambient air, PA devices essentially require the implementation of algorithmic models,

https://doi.org/10.5194/egusphere-2023-1010
Preprint. Discussion started: 9 June 2023

such as CoNRad, which are able to compute the relaxation cascade of PA signal generation, in order to provide reliable CH_4 concentration.

Code availability. The source code is available upon reasonable request. Please contact Max Müller (max.mueller@oth-regensburg.de) or Thomas Rück (thomas.rueck@oth-regensburg.de)

Data availability. For data related to this paper please contact Max Müller (max.mueller@oth-regensburg.de)

https://doi.org/10.5194/egusphere-2023-1010
Preprint. Discussion started: 9 June 2023

Appendix A: appendix

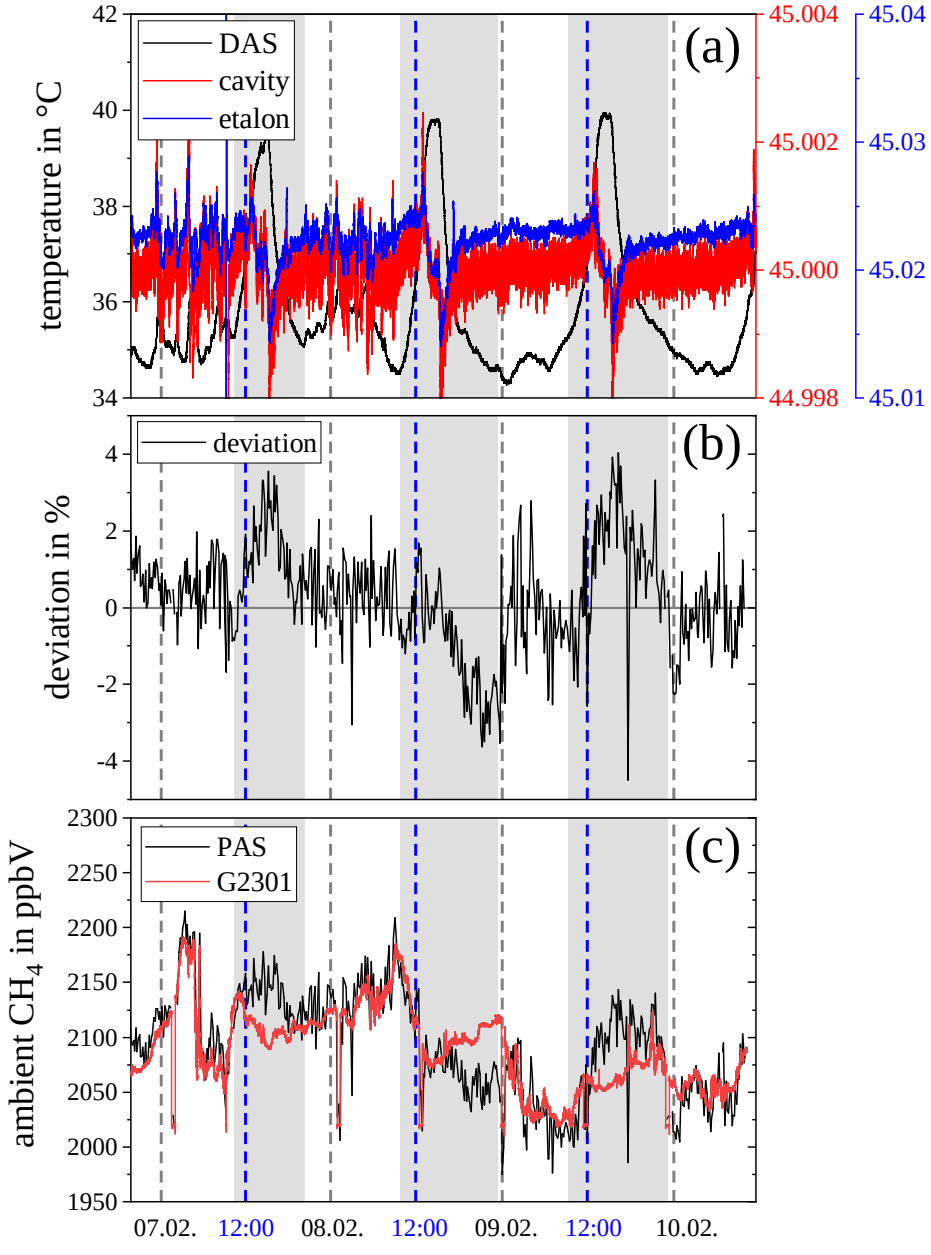

Figure A1. Comparison of data acquisition system (DAS), cavity and etalon temperature (a) of the Picarro G2301 CRDS over time, with the measured percentage deviation (b) and CH_4 reading (c). The temperature spikes (grey highlighted areas) seem to correlate with the strongest deviations. The blue dashed lines indicate noon, which leads to the assumption that such spikes in temperature may be caused by direct sun exposure of the device.

https://doi.org/10.5194/egusphere-2023-1010
Preprint. Discussion started: 9 June 2023

Author contributions. **Max Müller**: Conceptualization, Data curation, Investigation, Methodology, Software,Writing – original draft, Writing – review & editing. **Stefan Weigl**: Conceptualization, Data curation, Investigation, Methodology, Software,Writing – review & editing. **Jennifer Müller-Williams**: Conceptualization, Data curation, Investigation, Methodology, Writing – review & editing. **Matthias Lindauer**: Conceptualization, Data curation, Investigation, Methodology, Writing – review & editing. **Thomas Rück**: Methodology, Software, Validation, Funding acquisition, Writing – review & editing. **Simon Jobst**: Methodology, Software, Validation, Writing – review & editing. **Rudolf Bierl**: Funding acquisition, Project administration, Supervision, Validation, Writing – review & editing. **Frank-Michael Matysik**: Conceptualization, Methodology, Supervision, Validation, Writing – review & editing.

Competing interests. The authors declare that they have no conflict of interest.

Acknowledgements. This work was financially supported by the project PreSEDA funded by the German government and the Federal Ministry of Economic Affairs and Energy (BMWi). The funding code of PreSEDA is 03EN2028A.

https://doi.org/10.5194/egusphere-2023-1010
Preprint. Discussion started: 9 June 2023

References

Barreiro, N., Vellespi, A., Santiago, G., Slezak, V., and Peuriot, A.: Influence of oxygen on the resonant photoacoustic signal from methane excited at the $\nu 3$ mode, Applied Physics B, 104, 983–987, https://doi.org/https://doi.org/10.1007/s00340-011-4546-8, 2011.

Barreiro, N., Peuriot, A., Santiago, G., and Slezak, V.: Water-based enhancement of the resonant photoacoustic signal from methane–air samples excited at 3.3 μm, Applied Physics B, 108, 369–375, https://doi.org/https://doi.org/10.1007/s00340-012-5018-5, 2012.

Defratyka, S. M., Paris, J.-D., Yver-Kwok, C., Fernandez, J. M., Korben, P., and Bousquet, P.: Mapping Urban Methane Sources in Paris, France, Environmental Science & Technology, 55, 8583–8591, https://doi.org/10.1021/acs.est.1c00859, pMID: 34159780, 2021.

Dello Russo, S., Sampaolo, A., Patimisco, P., Menduni, G., Giglio, M., Hoelzl, C., Passaro, V. M., Wu, H., Dong, L., and Spagnolo, V.: Quartz-enhanced photoacoustic spectroscopy exploiting low-frequency tuning forks as a tool to measure the vibrational relaxation rate in gas species, Photoacoustics, 21, 100 227, https://doi.org/https://doi.org/10.1016/j.pacs.2020.100227, 2021.

Elefante, A., Giglio, M., Sampaolo, A., Menduni, G., Patimisco, P., Passaro, V. M., Wu, H., Rossmadl, H., Mackowiak, V., Cable, A., Tittel, F. K., Dong, L., and Spagnolo, V.: Dual-Gas Quartz-Enhanced Photoacoustic Sensor for Simultaneous Detection of Methane/Nitrous Oxide and Water Vapor, Analytical Chemistry, 91, 12 866–12 873, https://doi.org/10.1021/acs.analchem.9b02709, pMID: 31500409, 2019.

Elefante, A., Menduni, G., Rossmadl, H., Mackowiak, V., Giglio, M., Sampaolo, A., Patimisco, P., Passaro, V. M. N., and Spagnolo, V.: Environmental Monitoring of Methane with Quartz-Enhanced Photoacoustic Spectroscopy Exploiting an Electronic Hygrometer to Compensate the H2O Influence on the Sensor Signal, Sensors, 20, https://doi.org/10.3390/s20102935, 2020.

Giglio, M., Zifarelli, A., Sampaolo, A., Menduni, G., Elefante, A., Blanchard, R., Pfluegl, C., Witinski, M. F., Vakhshoori, D., Wu, H., Passaro, V. M., Patimisco, P., Tittel, F. K., Dong, L., and Spagnolo, V.: Broadband detection of methane and nitrous oxide using a distributed-feedback quantum cascade laser array and quartz-enhanced photoacoustic sensing, Photoacoustics, 17, 100 159, https://doi.org/https://doi.org/10.1016/j.pacs.2019.100159, 2020.

Gong, Z., Gao, T., Mei, L., Chen, K., Chen, Y., Zhang, B., Peng, W., and Yu, Q.: Ppb-level detection of methane based on an optimized T-type photoacoustic cell and a NIR diode laser, Photoacoustics, 21, 100 216, https://doi.org/https://doi.org/10.1016/j.pacs.2020.100216, 2021.

Hayden, J., Baumgartner, B., and Lendl, B.: Anomalous Humidity Dependence in Photoacoustic Spectroscopy of CO Explained by Kinetic Cooling, Applied Sciences, 10, https://doi.org/10.3390/app10030843, 2020.

Hunter, T. F., Rumbles, D., and Stock, M. G.: Photophysical processes in the vapour-phase measured by the optic-acoustic effect. Part 1.—The model and apparatus for the study of radiationless processes, J. Chem. Soc., Faraday Trans. 2, 70, 1010–1021, https://doi.org/10.1039/F29747001010, 1974.

Jackson, R. B., Down, A., Phillips, N. G., Ackley, R. C., Cook, C. W., Plata, D. L., and Zhao, K.: Natural Gas Pipeline Leaks Across Washington, DC, Environmental Science & Technology, 48, 2051–2058, https://doi.org/10.1021/es404474x, pMID: 24432903, 2014.

Kalkman, J. and van Kesteren, H.: Relaxation effects and high sensitivity photoacoustic detection of NO2 with a blue laser diode, Applied Physics B, 90, 197–200, https://doi.org/https://doi.org/10.1007/s00340-007-2895-0, 2008.

Lang, B., Breitegger, P., Brunnhofer, G., Valero, J., Schweighart, S., Klug, A., Hassler, W., and Bergmann, A.: Molecular relaxation effects on vibrational water vapor photoacoustic spectroscopy in air, Applied Physics B, 126, https://doi.org/https://doi.org/10.1007/s00340-020-7409-3, 2020.

Li, Y., Wang, R., Tittel, F. K., and Ma, Y.: Sensitive methane detection based on quartz-enhanced photoacoustic spectroscopy with a high-power diode laser and wavelet filtering, Optics and Lasers in Engineering, 132, 106 155, https://doi.org/https://doi.org/10.1016/j.optlaseng.2020.106155, 2020.

https://doi.org/10.5194/egusphere-2023-1010
Preprint. Discussion started: 9 June 2023

Li, Z., Liu, J., Si, G., Ning, Z., and Fang, Y.: Design of a high-sensitivity differential Helmholtz photoacoustic cell and its application in methane detection, Opt. Express, 30, 28 984–28 996, https://doi.org/10.1364/OE.465161, 2022.

Menduni, G., Sgobba, F., Russo, S. D., Ranieri, A. C., Sampaolo, A., Patimisco, P., Giglio, M., Passaro, V. M., Csutak, S., Assante, D., Ranieri, E., Geoffrion, E., and Spagnolo, V.: Fiber-Coupled Quartz-Enhanced Photoacoustic Spectroscopy System for Methane and Ethane Monitoring in the Near-Infrared Spectral Range, Molecules, 25, https://doi.org/10.3390/molecules25235607, 2020.

Miklós, A., Hess, P., and Bozóki, Z.: Application of acoustic resonators in photoacoustic trace gas analysis and metrology, Review of Scientific Instruments, 72, 1937–1955, https://doi.org/10.1063/1.1353198, 2001.

Müller, M., Rück, T., Jobst, S., Pangerl, J., Weigl, S., Bierl, R., and Matysik, F.-M.: An Algorithmic Approach to Compute the Effect of Non-Radiative Relaxation Processes in Photoacoustic Spectroscopy, Photoacoustics, 26, 100 371, https://doi.org/https://doi.org/10.1016/j.pacs.2022.100371, 2022.

Pangerl, J., Müller, M., Rück, T., Weigl, S., and Bierl, R.: Characterizing a sensitive compact mid-infrared photoacoustic sensor for methane, ethane and acetylene detection considering changing ambient parameters and bulk composition (N2, O2 and H2O), Sensors and Actuators B: Chemical, 352, 130 962, https://doi.org/https://doi.org/10.1016/j.snb.2021.130962, 2022.

Qiao, Y., Tang, L., Gao, Y., Han, F., Liu, C., Li, L., and Shan, C.: Sensitivity enhanced NIR photoacoustic CO detection with SF6 promoting vibrational to translational relaxation process, Photoacoustics, 25, 100 334, https://doi.org/https://doi.org/10.1016/j.pacs.2022.100334, 2022.

Rück, T., Müller, M., Jobst, S., Weigl, S., Pangerl, J., Bierl, R., and Matysik, F.-M.: Digital Twin of a photoacoustic trace gas sensor for monitoring methane in complex gas compositions, Sensors and Actuators B: Chemical, 378, 133 119, https://doi.org/https://doi.org/10.1016/j.snb.2022.133119, 2023.

Schilt, S., Besson, J.-P., and Thevenaz, L.: Near-infrared laser photoacoustic detection of methane: the impact of molecular relaxation, Applied Physics B, 82, 319–328, https://doi.org/https://doi.org/10.1007/s00340-005-2076-y, 2006.

von Fischer, J. C., Cooley, D., Chamberlain, S., Gaylord, A., Griebenow, C. J., Hamburg, S. P., Salo, J., Schumacher, R., Theobald, D., and Ham, J.: Rapid, Vehicle-Based Identification of Location and Magnitude of Urban Natural Gas Pipeline Leaks, Environmental Science & Technology, 51, 4091–4099, https://doi.org/10.1021/acs.est.6b06095, pMID: 28326761, 2017.

Wysocki, G., Kosterev, A., and Tittel, F.: Influence of molecular relaxation dynamics on quartz-enhanced photoacoustic detection of CO2 at λ =2 μm, Applied Physics B, 85, 301–306, https://doi.org/https://doi.org/10.1007/s00340-006-2369-9, 2006.

Xiao, H., Zhao, J., Sima, C., Lu, P., Long, Y., Ai, Y., Zhang, W., Pan, Y., Zhang, J., and Liu, D.: Ultra-sensitive ppb-level methane detection based on NIR all-optical photoacoustic spectroscopy by using differential fiber-optic microphones with gold-chromium composite nanomembrane, Photoacoustics, 26, 100 353, https://doi.org/https://doi.org/10.1016/j.pacs.2022.100353, 2022.